

International Journal of Modern Physics E  
 © World Scientific Publishing Company

## SEMICLASSICAL DESCRIPTION OF EXOTIC NUCLEAR SHAPES

X. VIÑAS<sup>a</sup>, M. CENTELLES<sup>a</sup> and M. WARDA<sup>a,b</sup>

<sup>a</sup> *Departament d'Estructura i Constituents de la Matèria and Institut de Ciències del Cosmos, Facultat de Física, Universitat de Barcelona, Diagonal 647, 08028 Barcelona, Spain*

<sup>b</sup> *Katedra Fizyki Teoretycznej, Uniwersytet Marii Curie-Skłodowskiej, ul. Radziszewskiego 10, 20-031 Lublin, Poland*

Received (received date)

Revised (revised date)

Exotic nuclear structures such as bubbles and tori are analyzed through semiclassical extended Thomas-Fermi calculations with the Skyrme force SkM\*. The variational equations for neutron and proton densities are solved fully self-consistently in spherical (bubbles) and cylindrical (tori) symmetries. The possible existence of bubble configurations in some astrophysical scenarios is discussed. The stability of toroidal structures against change of quadrupole moment is studied. A global minimum of the energy is found in heavy toroidal nuclei.

### 1. Introduction

The idea that stable or metastable nuclei could exist in the form of spherical bubbles was suggested many years ago.<sup>1,2,3</sup> In the seventies Wong<sup>4</sup> investigated the stability of exotic shapes, namely spherical bubbles and tori, in the framework of the liquid drop model (LDM)<sup>5</sup> with Strutinsky shell corrections.<sup>6</sup> Wong found that within the LDM bubble and toroidal structures were unstable against some deformations, but they could be stabilized with the help of shell corrections. He addressed his study to known nuclei near the the  $\beta$ -stability valley. More recently, Dietrich and Pomorski<sup>7</sup> have carried out a similar analysis for bubble nuclei with large mass numbers. They have found stability islands for spherical bubbles in the range of mass numbers  $A$  between 450 and 3000. Possible large bubble structures have also been analyzed within the mean-field approximation with the Hartree-Fock-Bogoliubov (HFB) theory and the DIS Gogny force.<sup>8,9</sup>

Semiclassical methods of Thomas-Fermi (TF) type are a powerful tool for the study of nuclear properties that smoothly vary with the number of particles  $A$ . Similarly to the LDM the TF methods are free of shell corrections, but they describe the nuclear surface in a consistent way.<sup>10</sup> As is known, the self-consistent density profiles at the pure TF level end at the classical turning point. This deficiency can be cured by using the extended Thomas-Fermi (ETF) method<sup>11,12</sup> which adds to the pure TF approach  $\hbar^2$  (and  $\hbar^4$ ) corrections coming from the non-commutativity between the position and momentum operators. The ETF approach allows to obtain

2 *X. Viñas, M. Centelles, M. Warda*

self-consistent density profiles with a fall-off similar to the one obtained with the mean field Hartree-Fock (HF) or HFB calculations.

The TF and ETF approaches are free of shell effects and replace the wave functions by the proton and neutron local densities as the main variables. This fact makes these approaches particularly useful for dealing with calculations with a very large number of particles or that involve the continuum (as the description of hot nuclei) where complete HF calculations may be extremely complicated.

Our aim in this paper is to study with some detail the ETF predictions for large spherical bubbles and toroidal distributions. It is a step towards a more complete description of these structures, that will imply to compute the shell energy with the same effective interaction used to calculate the ETF energy. In the second section we briefly outline the basic theory. In the third section we present our results for spherical bubbles and discuss the existence of two different density distributions with almost the same energy per particle for the same nucleus. Some attention is paid to the possibility that bubble structures can appear in model astrophysical scenarios. In the fourth section we analyze toroidal distributions in deformed ETF calculations constrained by a negative mass quadrupole moment. Our conclusions and outlook are given in the last section.

## 2. Basic theory

In this work we will use for our semiclassical study of bubble and toroidal structures the zero-range SkM\* interaction<sup>13</sup> which is known to give realistic fission barriers in actinide nuclei.<sup>11</sup> This seems a reasonable choice for describing nuclear structures containing several hundreds of nucleons.

The Skyrme energy density functional can be written as:

$$\mathcal{E} = \mathcal{E}_{kin} + \mathcal{E}_{zr} + \mathcal{E}_{den} + \mathcal{E}_{fin} + \mathcal{E}_{so} + \mathcal{E}_{Coul}, \quad (1)$$

where  $\mathcal{E}_{kin}$  is the kinetic energy including the density-dependent effective mass,  $\mathcal{E}_{zr}$  and  $\mathcal{E}_{den}$  are the zero-range central and density-dependent terms which are functions of the neutron and proton densities  $\rho_n$  and  $\rho_p$  only,  $\mathcal{E}_{fin}$  depends on  $\nabla\rho_n$  and  $\nabla\rho_p$  and simulates the finite range of the effective nucleon-nucleon interaction, and finally  $\mathcal{E}_{so}$  and  $\mathcal{E}_{Coul}$  are the contributions to the energy density coming from the spin-orbit and Coulomb interactions, respectively.

In the semiclassical ETF approach up to  $\hbar^2$  order, the kinetic and spin-orbit energy densities are expressed as functionals of the local density as follows:

$$\begin{aligned} \mathcal{E}_{kin} = \sum_q \frac{\hbar^2 \tau_q}{2m_q^*} = \sum_q \frac{\hbar^2}{2m} f_q \tau_q = \sum_q \frac{\hbar^2}{2m} \left\{ \frac{3}{5} (3\pi^2)^{2/3} f_q \rho_q^{5/3} + \frac{1}{36} f_q \frac{(\nabla\rho_q)^2}{\rho_q} \right. \\ \left. - \frac{1}{3} \nabla f_q \cdot \nabla\rho_q - \frac{1}{12} \rho_q \frac{(\nabla f_q)^2}{f_q} + \frac{1}{2} \frac{\rho_q}{f_q} \left( \frac{2m}{\hbar^2} \right)^2 (\mathbf{W}_q)^2 \right\}, \quad (2) \end{aligned}$$

$$\mathcal{E}_{so} = -\frac{2m}{\hbar^2} \sum_q \frac{\rho_q}{f_q} (\mathbf{W}_q)^2, \quad (3)$$

where  $q = n, p$  for neutrons and protons, respectively. The ratio of the bare nucleon mass to the effective mass  $f_q$  and the spin-orbit potential  $\mathbf{W}_q$  are the standard expressions associated to the Skyrme energy density functional.<sup>11</sup>

The Coulomb energy density reads

$$\mathcal{E}_{Coul} = \frac{1}{2} \rho(\vec{r}) V_{Coul}(\vec{r}) - \frac{3}{4} e^2 \left(\frac{3}{\pi}\right)^{1/3} \rho_p^{4/3}(\vec{r}), \quad (4)$$

where we obtain the Coulomb potential  $V_{Coul}(\vec{r})$  by solving the discrete Poisson equation  $\Delta V_{Coul}(\vec{r}) = -4\pi\rho_p(\vec{r})$  using Gaussian elimination.

From the energy density (1) the variational Euler-Lagrange (EL) equations with the constraint on given number of neutrons and protons read

$$\frac{\delta}{\delta\rho_q} \int d\vec{r} (\mathcal{E} - \mu_n \rho_n - \mu_p \rho_p) = \frac{\partial\mathcal{E}}{\partial\rho_q} - \nabla \frac{\partial\mathcal{E}}{\partial\nabla\rho_q} + \Delta \frac{\partial\mathcal{E}}{\partial\Delta\rho_q} - \mu_q = 0. \quad (5)$$

The explicit expressions for the EL equations associated to the ETF energy functional up to  $\hbar^2$  order can be found in Ref. <sup>11</sup>. We solve the set of two coupled nonlinear second-order differential equations (5) by means of the so-called imaginary time-step method (ITSM).<sup>14</sup> The procedure we follow is described in detail in Appendix B of Ref. <sup>12</sup>. Our solution of Eqs. (5) is fully self-consistent, with no initial assumption about the shape of the neutron and proton density profiles which are obtained by solving Eqs. (5) once two boundary conditions are imposed. The EL equations of the ETF model have been solved self-consistently in spherical and cylindrical coordinates using the ITSM<sup>15</sup>. The deformed ETF model has been successfully applied to the semiclassical study of fission barriers with non-relativistic<sup>11,16</sup> and relativistic<sup>17</sup> interactions.

### 3. Spherical bubbles

In the left panel of Fig. 1 we display the neutron and proton density profiles of a nuclear system with  $N = 560$  neutrons and  $Z = 240$  protons as a representative example of bubble nuclei. In this case there exist two solutions of the EL equations (5) with very close energy per nucleon. One of the solutions corresponds to a sort of hyperheavy nucleus with a reduced but finite central density, that are called semi-bubbles or unsaturated nuclei.<sup>8,9</sup> The other solution, a true bubble, corresponds to a distribution where nucleons are concentrated in a relatively thin layer around the surface of a sphere. Actually, for a given atomic number  $Z$ , there are several values of  $N$  for which both solutions, semi-bubbles and true bubbles, coexist, similarly to the shape coexistence phenomenon in normal nuclei in the actinide region. This is illustrated in Table 1 where the energy per nucleon as well as the neutron and proton chemical potentials are reported for the  $Z = 240$  isotopic chain from the

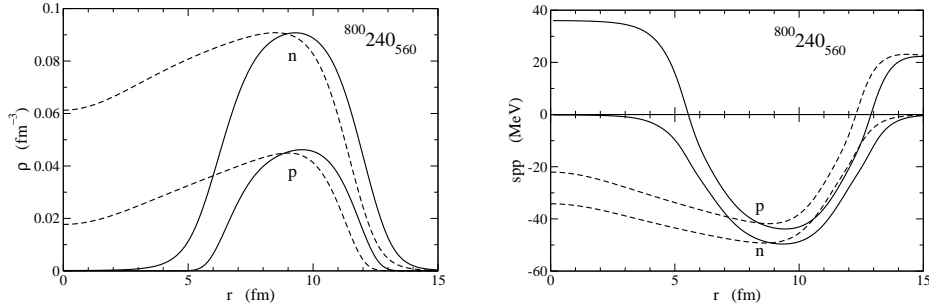
4 *X. Viñas, M. Centelles, M. Warda*

Fig. 1. Neutron and proton density profiles (left) and single-particle potentials (right) of a true bubble (solid line) and a semi-bubble (dashed line) with  $Z = 240$  protons and  $N = 560$  neutrons.

neutron to the proton drip lines of the bubble configuration. From Table 1 we see that semi-bubbles and true bubbles coexist in the range  $N = 524$  (proton drip line for semi-bubbles) up to  $N=576$ . Between  $N = 524$  and  $N = 498$  (proton drip line for true bubbles) only the true bubble solution is stable against proton emission, although solutions corresponding to unstable semi-bubbles (with a positive proton chemical potential) can also be found. Above  $N = 576$  and up to  $N = 620$  (neutron drip line for the true bubbles) we only obtain a true bubble solution.

From Table 1 we also realize that along the  $Z = 240$  isotopic chain the ground-state configuration corresponds to the true bubble solution. It has been found in HF calculations<sup>8,9</sup> that the situation is reversed for smaller values of  $Z$ , where the semi-bubble configuration becomes the ground state. We have checked that this also occurs in the ETF calculations. The energies per nucleon in semi-bubbles and bubbles reported in Table 1 are much smaller in absolute value than in normal nuclei. This is due to the fact that the binding mechanism of these huge nuclear clusters stems from a delicate balance between the increase of the surface energy and the reduction of the Coulomb energy obtained by putting the protons as separated as possible.

The neutron and proton single-particle potentials (spp) are displayed on the right panel of Fig. 1. Roughly, neutron and proton spp follow the corresponding densities. The neutron spp vanishes at the center of the nucleus for the true bubble solution while it is considerably reduced with respect to its minimal value in the semi-bubble case. The proton spp develops strong barriers at the center and at the outer part of the true bubbles, whereas the semi-bubble only develops the outer Coulomb barrier as expected.

Heavy-ion collisions at intermediate bombarding energies give strong evidences for the formation of highly excited nuclei. After some dissipation due to the pre-equilibrium emitted particles and rotation, the nucleus can reach an excited equilibrium state with some excitation energy  $E^*$ . This excited state can be described by means of a temperature  $T$  if the thermalization time is shorter than the typi-

Table 1. The energy per nucleon in MeV as well as neutron and proton chemical potentials in MeV of semi-bubbles and true bubbles for  $Z = 240$  isotopes.

${}^N Z$	semi-bubbles			bubbles		
	E/A	$\mu_n$	$\mu_p$	E/A	$\mu_n$	$\mu_p$
${}^{620}240$	—	—	—	-4.219	-0.003	-6.409
${}^{578}240$	—	—	—	-4.416	-0.696	-4.480
${}^{576}240$	-4.370	-0.576	-2.984	-4.424	-0.734	-4.380
${}^{560}240$	-4.441	-0.898	-2.135	-4.494	-1.047	-3.558
${}^{550}240$	-4.484	-1.115	-1.585	-4.535	-1.256	-3.025
${}^{524}240$	-4.587	-1.731	-0.076	-4.635	-1.848	-1.569
${}^{498}240$	-4.673	-2.428	1.543	-4.719	-2.516	-0.017

cal decay scale. This state is metastable with respect to nucleon emission and an artificial pressure has to be supplied in numerical calculations for avoiding that nucleons leave the nucleus. A possible way to do it is to put the nucleus in equilibrium with a nucleon gas representing the evaporated nucleons. It is assumed that this artificial pressure on the nucleus will not alter the actual physical picture of the excited nucleus. As soon as the temperature is not zero, the continuum states start to be occupied owing to the thermal Fermi factor. One way of isolating the hot nucleus of the continuum states was suggested by Bonche, Levit and Vautherin.<sup>18</sup> They found that at a given temperature and chemical potential, there exist two solutions of the HF equations. One corresponds to the nucleus in equilibrium with its evaporated gas, and the other one to the nucleon gas alone. They proposed to study the nucleus by means of a thermodynamical potential  $\tilde{\Omega}$  calculated as the difference of the grand potential  $\Omega$  associated to each one of these two solutions. This subtraction procedure can also be applied in the semiclassical TF or ETF approaches as shown by Suraud.<sup>19</sup>

It is worth to point out that when temperature increases shell corrections become less important and they nearly vanish around  $T \sim 2 - 3$  MeV.<sup>10</sup> This fact implies that semiclassical approaches of TF type, which are free of shell effects, are very well suited for dealing with calculations at high temperature. On the other hand, HF calculations have shown that there exists a limiting temperature  $T_{lim}$  beyond which normal nuclei become unstable because of the Coulomb interaction. When temperature grows, the surface energy decreases faster than the Coulomb contribution and, consequently, nucleons are driven out of the nucleus for a sufficiently high temperature.<sup>19</sup>

As far as at zero temperature spherical bubbles become stable against deformation due to shell effects, it could be expected that spherical bubbles should disappear around  $T \sim 2 - 3$  MeV when shell effects are washed out. However, using a simple model it has been shown that thermal effects could provide an extra stabilization against deformation.<sup>20</sup> We have performed thermal TF calculations with the semi-bubble  ${}^{500}180$  and with the true bubble  ${}^{900}274$  finding in both cases a lim-

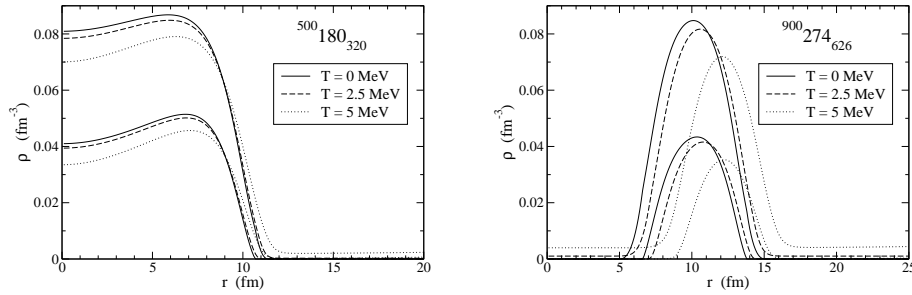
6 *X. Viñas, M. Centelles, M. Warda*

Fig. 2. Neutron and proton density profiles at  $T=0, 2.5$  and  $5$  MeV of bubbles containing  $500$  (left) and  $900$  (right) nucleons.

iting temperature of about  $5$  MeV. This limiting temperature in bubbles is smaller than the one found in normal nuclei, which lies in the range  $T_{lim} \sim 8 - 10$  MeV. This fact can be expected due to the large number of protons in the bubbles considered here which favor the Coulomb instability when temperature grows. At TF level the excitation energy per nucleon at the limiting temperature is  $3.40$  MeV/ $A$  for the semi-bubble  $^{500}_{320}180$  and  $2.06$  MeV/ $A$  for the true bubble  $^{900}_{626}274$ . This is in agreement with the fact that in normal nuclei the limiting excitation energy per nucleon decreases with increasing mass number. The fact that huge spherical bubbles cannot sustain a large amount of excitation energy has also been qualitatively discussed in Ref. <sup>7</sup>. In Fig. 2 the self-consistent TF neutron and proton density profiles corresponding to the liquid plus gas phase<sup>18,19</sup> at  $T = 0, 2.5$ , and  $5$  MeV are displayed. When temperature increases nucleons are pushed from the interior to the outer part of the system increasing the rms radius and the surface diffuseness of the density distributions.

The fact that isolated spherical bubbles that are stable against neutron and proton emission contain a large number of nucleons makes it difficult to obtain such nuclear clusters through heavy-ion collisions. As far as exotic nuclear shapes such as rods, pasta, etc. have been conjectured to occur in neutron stars<sup>21</sup>, it makes some sense the question whether exotic bubbles *as considered here* can exist in some astrophysical scenario. To investigate this we make use here of the simple approach developed in Ref. <sup>22</sup>. It is assumed that in nuclear matter at subnuclear densities the nuclei are located in a lattice which we treat in the spherical Wigner-Seitz (WS) approach. We consider a mixture of neutrons, protons, electrons and eventually neutrinos in  $\beta$  equilibrium inside each isolated WS cell assumed to be electrically neutral. In the regime that we are interested in, electrons are extremely relativistic and can be assumed to be uniformly distributed in the cell. We solve the problem self-consistently at TF level disregarding other particles, shell and pairing effects.

We consider first the outer crust of a neutron star where the WS cell contains a nuclear cluster surrounded by a neutron gas with an average density in the range

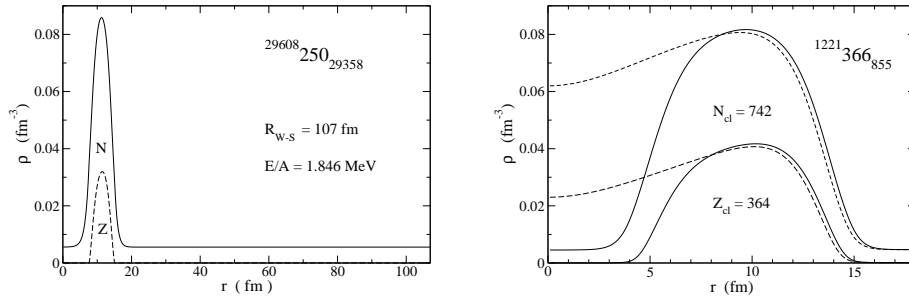


Fig. 3. Neutron and proton density profiles in a Wigner-Seitz cell in the outer crust of a neutron star (left) and in conditions prevailing during the gravitational collapse of massive stars (right).

$4.3 \times 10^{11} \text{ g/cm}^3 \lesssim \rho \lesssim 2.0 \times 10^{14} \text{ g/cm}^3$ .<sup>23</sup> In this scenario temperature is basically zero and there are no neutrinos trapped inside the WS cell. Fig. 3 (left panel) displays the neutron and proton density profiles obtained with our model assuming that the system with  $Z = 250$  is  $\beta$ -stable and the average density is  $\rho = 5.77 \times 10^{-3} \text{ fm}^{-3}$  in the WS cell. This two conditions allow to determine the radius of the WS cell which is  $R = 107 \text{ fm}$  and the number of nucleons inside the cell:  $A = 29608$ . The calculated energy per nucleon is 1.846 MeV which is close to the HF ground-state energy per nucleon at this average density.<sup>23</sup>

A different scenario concerns hot dense matter in conditions prevailing during the gravitational collapse of massive stars. One key ingredient for describing the collapse is just the EOS. In the relatively low density regime  $0.001 \text{ fm}^{-3} \lesssim \rho \lesssim 0.05 \text{ fm}^{-3}$  the most favored phase consists of nucleons congregated into nuclear clusters which can be huge ( $A \lesssim 1000$ ) and immersed in a free nucleon sea. In this case the WS cells contain neutrons, protons, electron and trapped neutrinos, again under the conditions of charge neutrality and  $\beta$ -equilibrium (for details see Ref. <sup>24</sup> and references therein). We calculate one possible point of the EOS at a constant entropy per nucleon  $S/A = 1k_B$ , as far as the collapse is fairly isentropic. The WS cell contains 855 neutrons and 366 protons corresponding to an average density  $\rho = 0.05 \text{ fm}^{-3}$  and a proton concentration  $Y_e = 0.3$ , which are typical conditions in this scenario.<sup>24</sup> The neutron and proton density profiles obtained by minimization of the *total* free energy  $F$  (including electrons and neutrinos) are displayed in Fig. 3 (right panel). We obtain two possible solutions with almost the same free energy per particle. One corresponds to a semi-bubble distribution ( $F/A = 28.86 \text{ MeV}$ ) and the other one to a true bubble embedded in a low density fluid ( $F/A = 28.73 \text{ MeV}$ ).

From these simple estimates in stellar media we conclude that spherical semi-bubbles and true bubbles could in principle exist in the considered astrophysical context. Whether these bubbles are stable against deformations demands further investigations.

#### 4. Toroidal structures

Long-lived nuclear structures beyond the island of stability may be reached if other topologies different from the sphere are considered. Simulations using Boltzmann-Uehling-Uhlenbeck (BUU) transport equations have shown that exotic shapes such as bubbles and tori could be created in central heavy-ion collisions.<sup>20</sup> Some effort has been addressed to find experimental evidences of the breakup of toroidal distributions produced in heavy-ion collisions.<sup>27</sup>

Nuclei of toroidal shape were first analyzed by Wong in the framework of the LDM plus Strutinsky shell corrections.<sup>4</sup> It was found that there exists a minimum of energy for such a type of shape which, however, is usually unstable against multifragmentation. Within mean-field theory using Skyrme forces the toroidal structure in superheavy nuclei was predicted by Nazarewicz et al.<sup>25</sup> More recently, axially symmetric toroidal superheavy nuclei with  $Z \geq 130$  have been analyzed by one of us within the HFB theory with the Gogny D1S force.<sup>26</sup> A global minimum of the binding energy in toroidal distributions is obtained by performing constrained HFB calculations with a relatively *large* and *negative* mass quadrupole moment  $Q_2$ . It is also found that for mass numbers  $A$  large enough, the superheavy toroidal nucleus becomes the ground state and it can be as much as 200 MeV more bound than the corresponding spherical nucleus.

We perform here deformed ETF calculations including  $\hbar^2$ -corrections with the SkM\* force to analyze semiclassically toroidal nuclei. The Weizsäcker term  $\frac{1}{36} f_q (\nabla \rho_q)^2 / \rho_q$  of the kinetic energy density given in Eq. (2) is multiplied by a factor 1.6 in such a way that the ETF surface energy calculated with the SkM\* interaction equals the HF value.<sup>16</sup>

Fig. 4 displays the potential energy surface (PES) as a function of the quadrupole mass moment  $Q_2$  for systems with  $^AZ = ^{298}122$ ,  $^{320}132$ ,  $^{352}144$  and  $^{416}164$ . Such systems would hypothetically be created in  $^{208}\text{Pb} + ^{90}\text{Zr}$ ,  $^{208}\text{Pb} + ^{112}\text{Sn}$ ,  $^{208}\text{Pb} + ^{144}\text{Sm}$  and  $^{208}\text{Pb} + ^{208}\text{Pb}$  collisions of stable nuclei, respectively. In all the analyzed cases we see that the PES consists of two branches that cross at a given value of  $Q_2$ . The crossing point is shifted to more negative values of  $Q_2$  when the mass number of the system increases. The dashed branches in the Fig 4. correspond to a compact oblate distribution and the solid ones to a toroidal shape. These two types of nuclear distributions can be seen in Fig. 5 where 2-dimensional plots of the self-consistent density of the nucleus  $^{416}164$  are displayed for the compact solution at  $Q_2 = -250$  b and for the toroidal structure at quadrupole moments  $Q_2 = -250$  b,  $-650$  b and  $-990$  b (ground state).

For the lightest system  $^{298}122$ , the ground state corresponds to a compact oblate shape with comparatively small negative deformation. However, when  $A$  and  $Z$  increase, the minimum point of the toroidal branch decreases and it becomes the ground state for the  $^{320}132$  system, as well as for the heavier systems. From Fig. 4 one also observes that when the mass and the charge of the system increase the ground-state energy is more negative as compared with the energy of the spherical



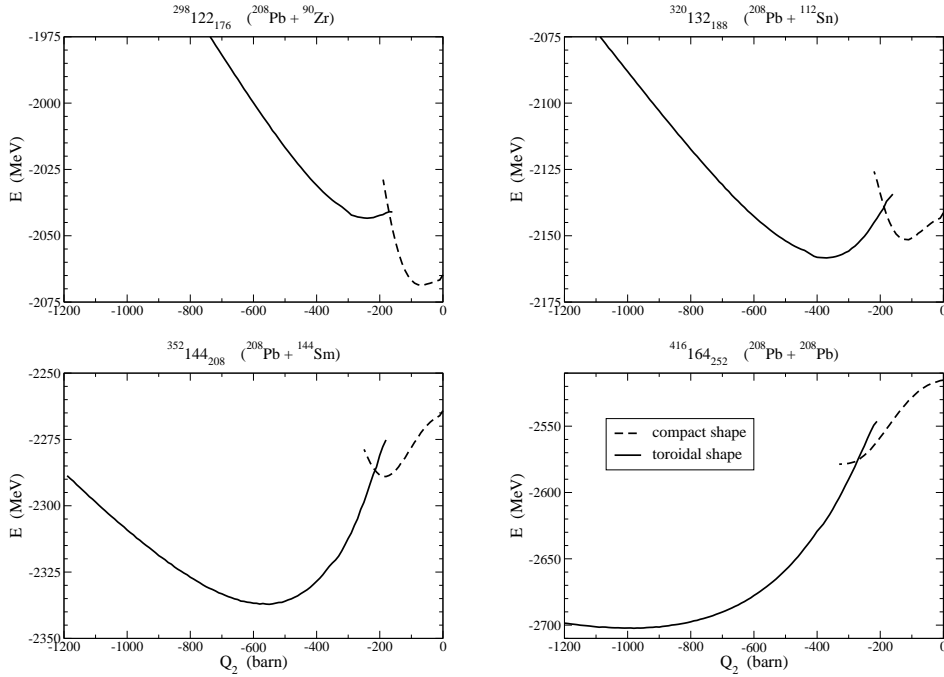


Fig. 4. The PES corresponding to  $^{298}_{122}176$ ,  $^{320}_{132}188$ ,  $^{352}_{144}208$  and  $^{416}_{164}252$  systems for negative values of the mass quadrupole moment  $Q_2$ .

solution ( $Q_2 = 0$ ). For heavy systems the minimum becomes more flat and its position is shifted to more negative values of the quadrupole moment making the toroidal nucleus unstable against multifragmentation. The PESs of toroidal nuclei calculated in the Skyrme ETF method (without shell corrections) are in qualitative agreement with previous findings in the mean-field HFB theory with the Gogny force, although there are differences in the absolute values of the binding energies of the system.<sup>26</sup>

In a small range of quadrupole momenta around the crossing  $Q_2$  values we find numerically two possible solutions of the EL equations (5) for the same value of  $Q_2$ . These two solutions have close binding energies. One of them belongs to the compact branch and the other one to the toroidal branch in Fig. 4. (This situation resembles the one discussed previously for spherical bubble distributions, where it is possible to find simultaneously semi-bubbles and true bubbles for some values of mass and atomic numbers.) In the case of the  $^{416}_{164}252$  system, the two solutions are found in the range  $-350 \lesssim Q_2 \lesssim -200$  b (see Fig. 4). Two-dimensional contour plots of the compact and toroidal density distributions at  $Q_2 = -250$  b for  $^{416}_{164}252$  are depicted in the upper panels of Fig. 5.

It is interesting to inspect the modification of the calculated PES induced by a finite temperature  $T$  and by the rotation of the torus around a radial axis with

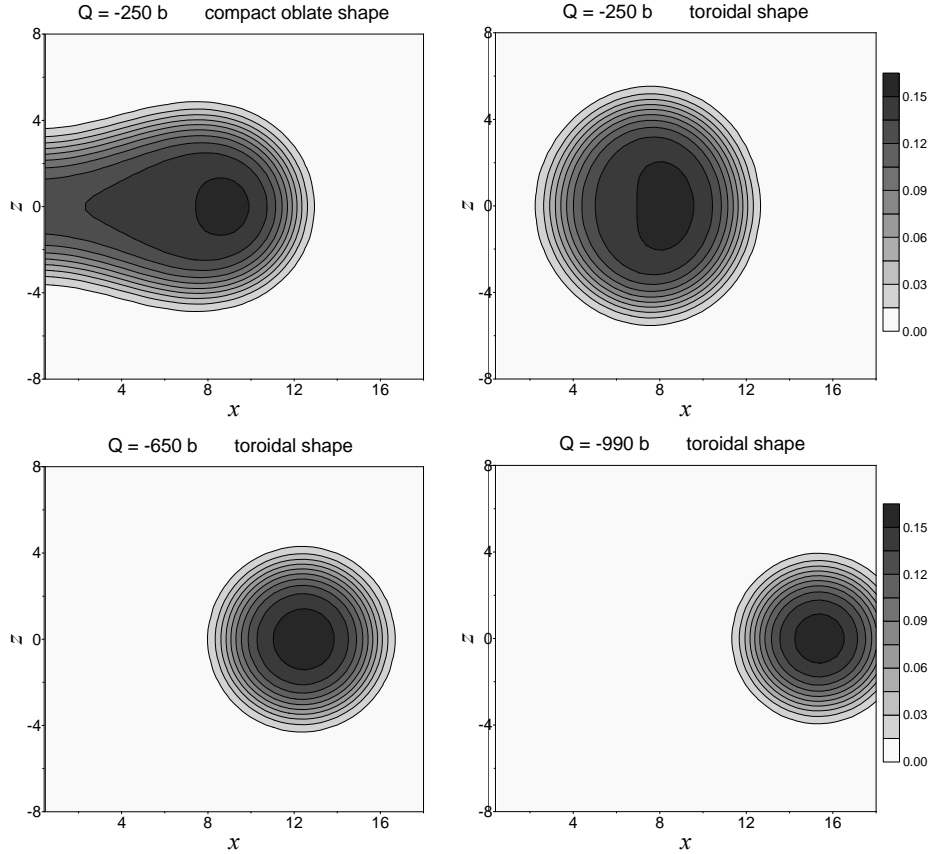
10 *X. Viñas, M. Centelles, M. Warda*

Fig. 5. Two-dimensional density plots in the  $xz$  plane for the nucleus  $^{416}_{164}$  at several mass quadrupole moments  $Q_2$ . The configurations are axially symmetric around the  $z$  direction.

angular momentum  $L_x$ . The stability of hot rotating toroidal structures was studied in the past by Wong<sup>28</sup> in the framework of the LDM. In the left panel of Fig. 6 we display our ETF results for the case of the  $^{416}_{164}$  system at  $T = 0$  and  $T = 1$  MeV, and when the system is rotating with angular momentum  $L_x = 150 \hbar$ . To simplify the figure, we use the same line style for the compact and toroidal branches of the PES in each studied case and do not draw the points in the crossing of the two branches.

One observes that for small values of  $T$  the excitation energy of the  $^{416}_{164}$  nucleus is roughly independent of the deformation  $Q_2$ . With a temperature  $T = 1$  MeV the energy is shifted upwards about 55–60 MeV along the whole PES. This value can be seen as the difference between the dashed and solid curves in the left panel of Fig. 6. We treat rotation in the rigid-body approximation as described in Ref. 17. The excitation energy gained by the  $^{416}_{164}$  system under rotation is more important for more compact (i.e. less deformed) distributions, as it can be expected

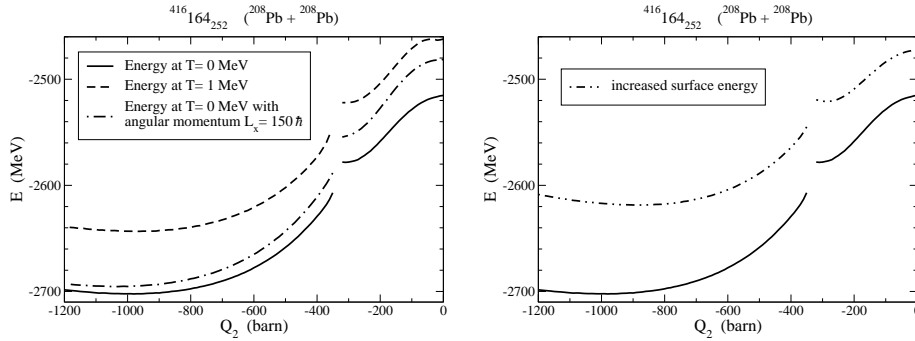


Fig. 6. Thermal and rotational (left) and surface energy (right) effects on the PES of the  $^{416}_{164}$  nucleus as a function of the mass quadrupole moment  $Q_2$ .

from the reduction of the rigid-body moment of inertia when  $Q_2$  increases (i.e. is less negative). In the present example, the energy gain of the system with angular momentum  $L_x = 150 \hbar$  with respect to the non-rotating system is around 30 – 35 MeV in the compact branch of the PES, while it decreases from about 20 MeV at  $Q_2 = -350$  b to only 7 MeV in the region around the minimum of the PES.

It is to be noted that the PES of toroidal nuclei depends on the value of the surface energy associated with the nuclear interaction. To exemplify this, we display in the right panel of Fig. 6 the PES of the  $^{416}_{164}$  system obtained multiplying the Weizsäcker term in Eq. (2) by a factor of 2 (to reproduce the LDM fission barrier of  $^{240}\text{Pu}$ )<sup>16</sup> instead of by the 1.6 factor used in the previous calculations. It can be seen that in this case the minimum exhibited by the PES is more marked and shifted towards more compact (less negative  $Q_2$ ) configurations. Consequently, it is expected that nuclear forces with large surface energy make toroidal nuclei more stable against multifragmentation.

## 5. Summary and outlook

In this work exotic nuclear shapes, namely bubbles and tori, containing several hundreds of nucleons are analyzed by means of the semiclassical extended Thomas-Fermi method and the Skyrme force SkM\*. Calculations are performed by solving fully self-consistently the variational Euler-Lagrange equations in spherical and axial symmetries. The ETF method incorporates in a consistent way the description of the nuclear surface and is free of shell effects. Although shell effects are crucial for the stability against deformation of these huge and exotic nuclear clusters, important information about the smooth variation with the number of particles of some global properties can be obtained from the semiclassical analysis.

As it happens in the HF calculations, for some neutron and proton numbers two different solutions of the ETF equations, namely semi-bubbles and true bubbles, are obtained. For a large enough number of nucleons the true bubbles are the

structure with minimal energy. We have also explored thermal effects in spherical bubbles. In this picture, spherical bubbles can exist at temperatures above the one for which shell effects disappear but with a limiting temperature smaller than for normal nuclei. Using a simplified model we have also explored the possible existence of spherical bubbles in astrophysical scenarios. From a semiclassical point of view it is found that semi-bubbles and true bubbles could exist in the outer crust of neutron stars and in hot and dense stellar matter in conditions prevailing during the gravitational collapse of massive stars.

We have performed deformed Extended Thomas-Fermi calculations for toroidal distributions of nucleons. Threshold values of the mass and atomic numbers exist beyond which toroidal nuclei become the ground state of the system. With increasing mass and charge the ground state of toroidal nuclei is more deformed and more bound with respect to the spherical solution, undergoing ultimately decay by multifragmentation. Effects of temperature, rotation and value of the surface energy on the PES of tori have also been discussed.

The semiclassical study presented here is a step towards a consistent description of bubbles and tori which has to include shell corrections computed from the semiclassical single-particle potentials. In this way it is expected to obtain a quantal description of these exotic nuclear clusters that will allow to know separately the smoothly varying and the oscillatory parts of some nuclear properties. The preliminary results obtained in astrophysical scenarios are very encouraging. An important point is to investigate the stability against deformation of bubbles embedded in a gas containing nucleons, electrons and neutrinos.

### Acknowledgments

Work supported in part by Grants No. FIS2005-03142 from MEC (Spain) and FEDER, No. 2005SGR-00343 from DGR (Generalitat de Catalunya) and No. N202 179 31/3920 from MNiSW (Poland).

### References

1. H. A. Wilson, *Phys. Rev.* **69**, 538 (1946).
2. J. A. Wheeler, Notebook, 1950, unpublished.
3. P. Siemens and H.A. Bethe, *Phys. Rev. Lett.* **18**, 704 (1967).
4. C. Y. Wong, *Ann. of Phys.* (NY) **79**, 319 (1973).
5. W. D. Myers and W. J. Swiatecki, *Ann. of Phys.* (NY) **55**, 395 (1969); *Ann. of Phys.* (NY) **84**, 186 (1974).
6. M. Brack, J. Damgaard, A. J. Jensen, H. C. Pauli, V. M. Strutinsky and C. Y. Wong, *Rev. Mod. Phys.* **44**, 320 (1972).
7. K. Dietrich and K. Pomorski, *Phys. Rev. Lett.* **80**, 37 (1997); *Nucl. Phys.* **A637**, 175 (1997).
8. J. Dechargé, J. F. Berger, K. Dietrich and M. S. Weiss, *Phys. Lett.* **B451**, 275 (1999).
9. J. Dechargé, J. F. Berger, M. Girod and K. Dietrich, *Nucl. Phys.* **A716**, 55 (2003).
10. M. Brack and P. Quentin, *Phys. Lett.* **B52**, 159 (1974); *Phys. Lett.* **B56**, 421 (1975); *Nucl. Phys.* **A361**, 35 (1981).

11. M. Brack, C. Guet and H. B. Håkansson, *Phys. Rep.* **123**, 275 (1985).
12. M. Centelles, M. Pi, X. Viñas, F. Garcias and M. Barranco, *Nucl. Phys.* **A510**, 397 (1990).
13. J. Bartel, P. Quentin, M. Brack, C. Guet and H. B. Håkansson, *Nucl. Phys.* **A445**, 263 (1985).
14. K. T. R. Davies, H. Flocard, S. Krieger and M. S. Weiss, *Nucl. Phys.* **A342**, 11 (1980).
15. D. Dalili, J. Nemeth and C. Ngô, *Z. Phys.* **A321**, 335 (1985).
16. F. Garcias, M. Barranco, J. Nemeth, C. Ngô and X. Viñas, *Nucl. Phys.* **A495**, 169c (1989).
17. M. Centelles, X. Viñas, M. Barranco, N. Ohtsuka, A. Faessler, D. T. Khoa and H. Müther, *Phys. Rev.* **C47**, 1091 (1993).
18. P. Bonche, S. Levit and D. Vautherin, *Nucl. Phys.* **A427**, 278 (1984).
19. E. Suraud, *Nucl. Phys.* **A462**, 109 (1987).
20. L. G. Moretto, K. Tso and G. J. Wozniak, *Phys. Rev. Lett.* **78**, 824 (1997).
21. C. J. Pethick and D. G. Ravenhall, *Annu. Rev. Nucl. Part. Sci.* **45**, 429 (1995).
22. Tapas Sil, J. N. De, S. K. Samaddar, X. Viñas, M. Centelles and S. K. Patra, *Phys. Rev.* **C66**, 045803 (2002).
23. J. W. Negele and D. Vautherin, *Nucl. Phys.* **A207**, 208 (1973).
24. M. Pi, X. Viñas, M. Barranco, A. Pérez-Canyellas and A. Polls, *Astron. Astrophys. Supp. Ser.* **64**, 439 (1986).
25. W. Nazarewicz, M. Bender, S. Ćwiok, P. H. Heenen, A.T. Kruppa, P.-G. Reinhard and T. Verste, *Nucl. Phys.* **A701**, 165c (2002).
26. M. Warda, *Int. J. Mod. Phys.* **E16**, 452 (2007).
27. D. O. Handzy et al.; *Phys. Rev.* **C51**, 2237 (1995); N. T. B. Stone et al., *Phys. Rev. Lett.* **78**, 2084 (1997); A. Sochoka et al., *Int. J. Mod. Phys.* **E17**, (2008) in press.
28. C. Y. Wong, *Phys. Rev.* **C17**, 331 (1978); **C30**, 1949 (1984); *Phys. Rev. Lett.* **55**, 1973 (1985); J. Zhang and C. Y. Wong, *Phys. Rev.* **C34**, 1094 (1986).